J Mater Sci: Mater Electron (2016) 27:4541–4550
DOI 10.1007/s10854-016-4329-4

Facile chemical synthesis of cobalt tungstates nanoparticles as high performance supercapacitor

Kourosh Adib[1,2] · Mehdi Rahimi-Nasrabadi[2,3] · Zolfaghar Rezvani[1] · Seied Mahdi Pourmortazavi[4] · Farhad Ahmadi[5] · Hamid Reza Naderi[6] · Mohammad Reza Ganjali[6]

Received: 19 October 2015 / Accepted: 10 January 2016 / Published online: 22 January 2016

Abstract Cobalt tungstate ($CoWO_4$) nanoparticles were synthesized by a chemical precipitation reaction in aqueous ambient involving direct addition of cobalt ion solution to the solution of tungstate reagent. Optimization of the synthesis procedure was carried out using Taguchi robust design as statistical method. In order to controllable, simple and fast synthesis of $CoWO_4$ nanoparticles, effects of some synthesis conditions such as reagents concentrations (i.e., cobalt and tungstate ions), flow rate of cobalt feeding and temperature of the reactor on the particle size of synthesized $CoWO_4$ were investigated by the aid of an orthogonal array (OA_9). The results of optimization process showed that $CoWO_4$ nanoparticles could be prepared by controlling the effective parameters and at optimum conditions of synthesis procedure, the size of prepared $CoWO_4$ particles was about 55 nm. Chemical composition and microstructure of the prepared $CoWO_4$ nanoparticles were characterized by means of XRD, SEM, TEM, FT-IR spectroscopy, UV–Vis spectroscopy and fluorescence. The supercapacitive behavior of the $CoWO_4$ electrode has been investigated by cyclic voltammetry, galvanostatic charge/discharge and electrochemical impedance spectroscopy. The $CoWO_4$ electrode indicates high specific capacitance of 378 F g^{-1} at scan rate of 2 mV s^{-1} in 2.0 M H_2SO_4 electrolyte. Therefore, the prepared electrode could be potential electrode materials for supercapacitors. Moreover, an excellent rate performance, good capacitance retention (~95.5 %) was also observed during the continuous 4000 cycles.

1 Introduction

In today's world, electrochemical supercapacitors (ESs) could be considered as one of the most important energy storage devices for a larger number of power portable electronics and electrical vehicles. They can be classified into two major groups based on the charge-storage mechanisms in them, electrical double-layer capacitors (EDLCs) and pseudocapacitors [1–4]. In fact, EDLCs store charges in the double layer of the electrode–electrolyte interface [5]. However, for enhancing specific capacitance of EDLCs, various carbon-based materials have been used, which have a large specific area [6]. The second group, pseudocapacitors, could have an individual capacitance due to their electrochemically active materials through rapid and faradic redox reaction. Numerous materials are used in construction of them, such as transition metal oxides [7], and conductive polymers [8]. ESs based on metal oxides, as electroactive materials are attracting great attention due to the low cost of the raw material, excellent electrochemical performance, and environmental compatibility [7]. Recently, numerous studies done on mixed metal oxide nanoparticles as

✉ Mehdi Rahimi-Nasrabadi
rahiminasrabadi@gmail.com

1 Department of Chemistry, Azarbaijan Shahid Madani University, Tabriz, Iran

2 Nano-Science Center, Imam Hossein University, Tehran, Iran

3 Faculty of Pharmacy, Baghiatallah University of Medical Sciences, Tehran, Iran

4 Faculty of Material and Manufacturing Technologies, Malek Ashtar University of Technology, Tehran, Iran

5 Department of Medicinal Chemistry, School of Pharmacy-International Campus, Iran University of Medical Sciences, Tehran, Iran

6 Center of Excellence in Electrochemistry, University of Tehran, Tehran, Iran

electroactive materials for ESs [9, 10]. Among the different mixed metal oxide studied, tungstates of transition are the most promising materials which shows superior supercapacitive performance with good rate capability, large specific capacitance, and excellent cyclic performance [11–16].

Transition metal tungstates (M^{2+} = Mn, Fe, Co, Ni, Cu, Zn) represent a most versatile groups of inorganic functional materials. Normally, $CoWO_4$ a member of the wolframite structure with monoclinic symmetry, space group P2/c. In wolframite structure, six oxygen atoms are surrounded each of the tungsten atoms [17]. Nanosize transition metal tungstates are among the materials with exciting fluorescent, laser, piezoelectric, ferroelectric and ferroelastic properties. Some of the metal tungstates are more unusual due to their particular electrical and magnetic properties [18]. Among them $CoWO_4$ attracted a lot of attention for photoluminescence, optoelectronics devices, pigment additives, microwave dielectric ceramics, scintillating material, microwave dielectrics and catalysis [19]. A range of methods including molten salt method [19], hydrothermal and solvothermal processes [20], spray pyrolysis [21], polymeric precursor method [22] have been used to prepare nanocrystalline cobalt tungstate with average diameters of 20–150 nm. Clearly each route has its own advantages and disadvantages, and hence choosing a proper technique for the preparation of the product requires the consideration of several aspects including the complexity, cost-affectivity, time etc.

In this work, the effect of process parameters are determining on the particle size of $CoWO_4$ and their optimization to prepare $CoWO_4$ nanoparticles by precipitation reaction. Afterward, the supercapacitive properties of the $CoWO_4$ electrode were examined by cyclic voltammetry (CV), continuous cyclic voltammetry (CCV), galvanostatic charge/discharge, and electrochemical impedance spectroscopy (EIS). Also, Structural and chemical characterization of the prepared salt nanoparticles was another aim of this investigation.

2 Experimental

2.1 Materials and methods

Analytical grade hydrates salts of sodium tungstate and cobalt nitrate as reagents were used as received from Merck Company (Germany). The cobalt tungstate particles were synthesized via precipitation reaction occurred between the reagents by direct addition of Co^{2+} aqueous solution with various concentrations and different feeding flow rates to the tungstate aqueous solution under vigorous stirring and various temperatures of reactor. After completion of the precipitation reaction, the precipitated cobalt tungstate particles were filtered and washed three times with distilled water. The product was then washed with ethanol and dried at 75 °C during 120 min. Optimization of the synthesis procedure experimental parameters was carried out by the aid of Taguchi robust design. Several variables, i.e., reagents concentrations (cobalt and tungstate ions), feeding flow rate of the cobalt reagent to the tungstate solution and temperature of the reactor were investigated as detailed in Table 1.

Scanning electron micrograms (SEMs) were acquired using a Philips XL30 series instrument using a gold film (prepared by a Sputter Coater model SCD005 made by BAL-TEC (Switzerland)) for loading the dried particles onto the instrument. Transmission electron microscope (TEM) image was obtained using a Ziess-EM900 scanning electron microscope. The sample preparation was performed by loading the sample on a Cu-carbon coated grid. The XRD of the samples was acquired using a Rigaku D/max 2500 V diffractometer equipped with a graphite monochromator and a Cu target. The IR spectra were

Table 1 Assignment of the factors and levels of the experiments by using an OA_9 (3^4) matrix and mean width of cobalt tungstate produced

Experiment number	Co^{2+} concentration (M)	WO_4^{2-} concentration (M)	Co^{2+} feed flow rate (mL/min)	Temperature (°C)	Diameter of $CoWO_4$ particles (nm)
1	0.005	0.005	2.5	0	100
2	0.005	0.01	10.0	30	60
3	0.005	0.1	40.0	60	55
4	0.01	0.005	10.0	60	82
5	0.01	0.01	40.0	0	68
6	0.01	0.1	2.5	30	64
7	0.1	0.005	40.0	30	80
8	0.1	0.01	2.5	60	62
9	0.1	0.1	10.0	0	68

recorded through a Bruck Equinox 55 IR spectrophotometer using the KBr pellet method.

2.2 Electrochemical study

The electrochemical test was performed as follows: The as-prepared $CoWO_4$ powder were mixed with acetylene black, graphite, and poly(tetrafluoroethylene) in a mass ratio of 65:20:10:5 and dispersed in ethanol to produce a homogeneous paste. Then the slurry was pressed onto a piece of stainless steel current collector under a pressure of 20 MPa. Each electrode contained about 3 mg of electroactive material and had a geometric surface area of about 1 cm^2. Finally, the fabricated electrode was dried at 80 °C for 4 h in a vacuum oven.

All the electrochemical measurements were performed under a three-electrode cell at room temperature: the stainless steel grid coated with electroactive materials was used as the working electrode, and a Pt foil (1 cm^2) and a Ag/AgCl (saturated KCl) electrode were used as the counter and reference electrodes, respectively; 2.0 M H_2SO_4 aqueous solution was prepared as the electrolyte. The Cyclic voltammetry (CV) and CCV measurements Galvanostatic charge/discharge, and electrochemical impedance spectroscopy (EIS) were carried out by an Autolab PGSTAT 204 type electrochemical workstation.

3 Results and discussion

3.1 Nanoparticles preparation and optimization of procedure

In the present investigation similar to the other simultaneous optimization methods, the required experiments for optimization of the parameters were carried out based on the previously designed plan [23–25]. After performing the designed experiments (shown in Table 1), the experimental results were collected in the last column of this table and then the calculations and evaluation of them was performed to obtaining the optimum conditions for preparation of cobalt tungstate nanoparticles.

The studied variables in this research were including: reagents aqueous solutions concentrations (i.e., Co^{2+} and WO_4^{2-}), cobalt solution feeding flow rate to the WO_4^{2-} solution, and the temperature of the solution in the reactor. The selected levels for these variables are presented in Table 1. The prepared $CoWO_4$ samples according to the designed experiments (Table 1) were characterized by SEM and some of these images correspond to four of these experiments are shown in Fig. 1 for comparison. As seen in the figure and size of particles presented in the last column of Table 1, particle size of the prepared $CoWO_4$ depends on the operation conditions. Meanwhile, the calculated average particle size of cobalt tungstate correspond to the effect of each variable at any level [26, 27] are presented in the Fig. 2. As could be seen in this figure, particle size of $CoWO_4$ particles varies with changing the level of each factor. The $CoWO_4$ particles obtained by precipitation reaction under various conditions (according Table 1) were spherical shaped; while their diameter differs regarding on the reaction conditions. As shown in Table 1 the smallest values of particle size of cobalt tungstate (55 nm) were obtained by runs 3 while the largest values of particle size of product (100 nm) were produced in run 1. In this work, concentrations of Co^{2+} and WO_4^{2-} aqueous solutions were varied at three different values (0.005, 0.01, 0.1 mol/L) to investigate the effect of reagents concentrations on the size of produced $CoWO_4$ particles. Figure 2a shows that 0.1 M, as the concentration of cobalt and tungstate ion solutions, is optimum concentration for production $CoWO_4$ fine particles. As seen in Fig. 2b, among the studied values of feeding flow rates (2.5, 10, 40 mL/min) for addition of cobalt reagent to the reactor containing tungstate solution 40 mL/min is the best flow rate for synthesis of ultrafine particles of $CoWO_4$. On the other hand, this figure confirms that the best temperature for synthesis of $CoWO_4$ particle with minimum size is 60 °C.

After determination the average response of any factor at each level (Fig. 2), analysis of variance (ANOVA) was applied to evaluate the significance (at 90 % confidence interval) of the studied factors on the definition particle size of $CoWO_4$. Table 2 presents the results of ANOVA which confirm that except the concentration of cobalt solution, other studied variables (tungstate ion concentration, feeding flow rate, and reactor temperature) have significant effects in controlling the particle size of $CoWO_4$. The probable interactions between the studied variables in this research were not considered. Considering the average effect of factors at their levels (Fig. 2) and the results of ANOVA (Table 2) results in optimum conditions for synthesis of $CoWO_4$ nanoparticles with smaller diameter via direct precipitation reaction as: 0.1 mol/L concentration of tungstate ion, 40 mL/min as cobalt reagent feeding flow rate for its addition to the tungstate solution and 60 °C as reactor temperature. The optimum performance of the procedure for preparation of $CoWO_4$ nanoparticles with smallest diameter could be estimated using following expression taken from Taguchi method [28]:

$$Y_{opt} = \frac{T}{N} + \left(C_x - \frac{T}{N}\right) + \left(F_y - \frac{T}{N}\right) + \left(T_z - \frac{T}{N}\right)$$

in which T/N represents the average size of $CoWO_4$ particles calculated from the results shown in the last column of Table 1 + contribution of C_X, F_y, and T_z above average performance; while, T is the grand total of all particle size

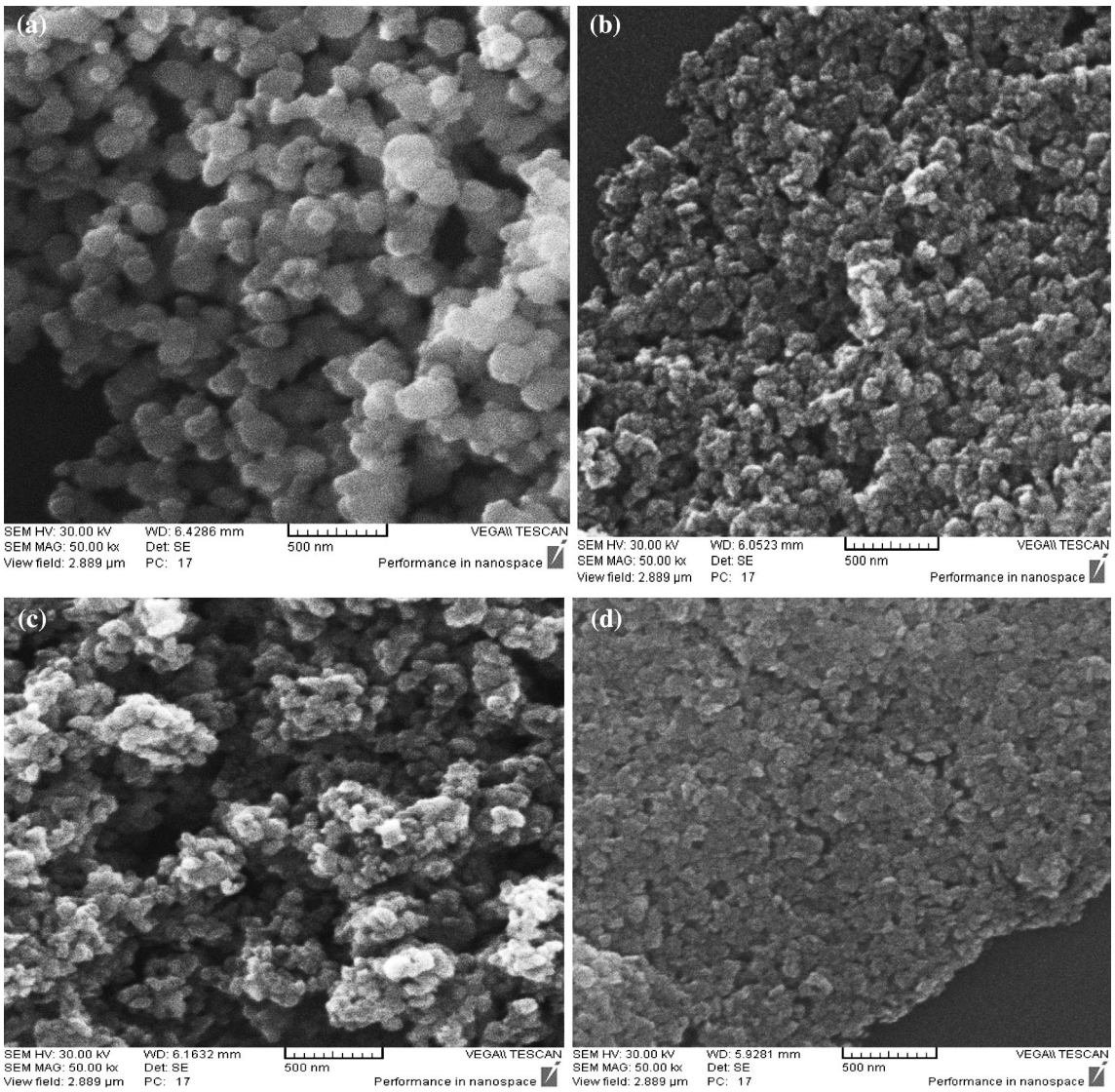

Fig. 1 SEM images of $CoWO_4$ nanoparticles obtained at different runs by precipitation method: **a** run 1, **b** run 3, **c** run 4, and **d** run 9

results in Table 1, N is the number of trials in this table, Y_{opt} is size of $CoWO_4$ particles at optimum conditions of synthesis procedure, C_X, F_y, and T_z are optimum concentration of WO_4^{2-}, cobalt ion feeding flow rate, and reactor temperature, respectively. The confidence interval (CI) for the particle size prepared under the optimum conditions is calculated through the following equation [29]:

$$CI = \pm\sqrt{\frac{F_\alpha(f_1,f_2)V_e}{n_e}}$$

where, V_e represents the variance of error shown in Table 2, $F_\alpha(f_1, f_2)$ is variance ratio for degree of freedom (DOF), f_1 and f_2 are considered at the level of significance α (here, $\alpha = 90$ %), $f_1 =$ DOF for mean (which always equals 1), $f_2 =$ DOF for error term in Table 2, $n_e =$ number of equivalent replications which is obtained by the following expression.

The confidence interval (CI) for the particle size prepared under the optimum conditions is calculated through the following equation

$$n_e = \frac{Number\ of\ experiments}{DOF\ of\ mean\ (always\ 1)\ +\ DOF\ of\ all\ factors\ used\ in\ estimation}$$

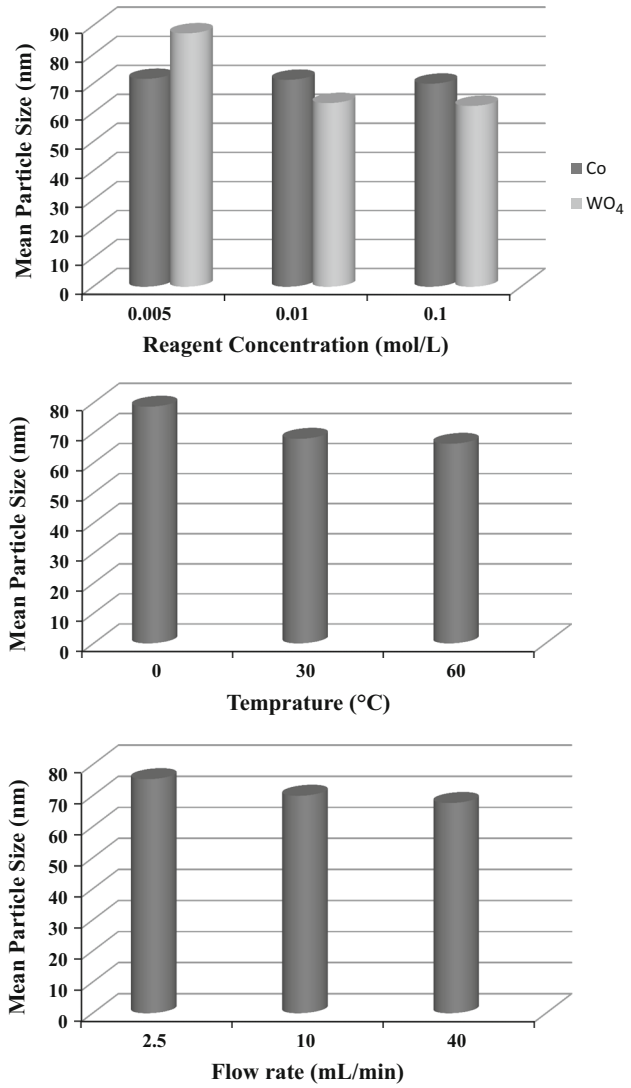

Fig. 2 Main effects for each variable of precipitation reaction on the diameter of $CoWO_4$ nanoparticles

The product size calculated for optimum conditions and *CI*, at a 90 % confidence level, were 54.3 ± 3.88 nm.

The third run in Table 1 include the optimum reaction conditions obtained from the results of ANOVA (0.1 mol/L concentration of tungstate ion, 40 mL/min as cobalt reagent feeding flow rate for its addition to the tungstate solution and 60 °C as reactor temperature). The acquired SEM images proved that the products obtained under these conditions (i.e., run 3) have an average diameter of about 55 nm (Fig. 1b) which is consistent with the calculated results. The results of the TEM analysis of the same product samples (Fig. 3) further confirmed their size and morphology, indicating the particles to be spherical and proving their average diameter of about 50 nm. The particles prepared under the experimental conditions of run 3 were further characterized through XRD, FT-IR, fluorescence and UV–Vis.

3.2 Characterization of cobalt tungstate nanoparticles

$CoWO_4$ nanoparticles were prepared by precipitation reaction at optimum conditions proposed by Taguchi method. This sample was characterized by X-ray powder diffraction (XRD) to evaluate its composition and purity. XRD pattern for the cobalt tungstate nanoparticles is shown in Fig. 4. The peaks of XRD pattern of the samples have a strong intensity and smoothed baseline which indicated that cobalt tungstate to have a crystalline structure with high purity. All the diffraction peaks are in very well consistent with the monoclinic wolframite structure from the PDF card 00-015-0867.

Formation of $CoWO_4$ and presence of the corresponding functional groups were also confirmed with FT-IR spectroscopy.

FT-IR spectra for the produced $CoWO_4$ nanoparticles before and after annealing of the sample at 600 °C are shown in Fig. 5. Figure 5a exhibits that the cobalt tungstate sample before annealing exhibits four wide absorption peaks at about 573.3, 727.2, 1633.5 and 3418.3 cm^{-1}. The FT-IR spectrum confirms presence of the moisture in cobalt tungstate sample. The peak at 3418.3 cm^{-1} corresponds to the stretching and bending vibrations of O–H and H–O–H of the water molecules that are absorbed on the surface of the sample [17, 30]. However, in the FT-IR spectrum of the annealed sample in Fig. 5b six absorption bands (at 466.3, 526.2, 611.7, 685.1, 818.7, 867.1 cm^{-1}) is

Table 2 ANOVA table for synthesis $CoWO_4$ particles using precipitation procedure by $OA_9(3^4)$ matrix with diameter of synthesized $CoWO_4$ particles (nm) as the response

Factor	Code	DOF	S	V	Pooled[a]			
					DOF	S′	F′	P′
Cobalt concentration (mol/L)	Co	2	4.67	2.33	–	–	–	–
Tungstate concentration (mol/L)	WO_4	2	1202.00	601.00	2	1202.00	257.6	76.4
Flow rate (mL/min)	F	2	92.67	46.33	2	92.67	19.9	5.6
Temperature (°C)	T	2	268.67	134.33	2	268.67	57.6	16.8
Error	E	–	–	–	2	4.67	–	1.2

[a] The critical value was at 90 % confidence level; pooled error results from pooling insignificant effect

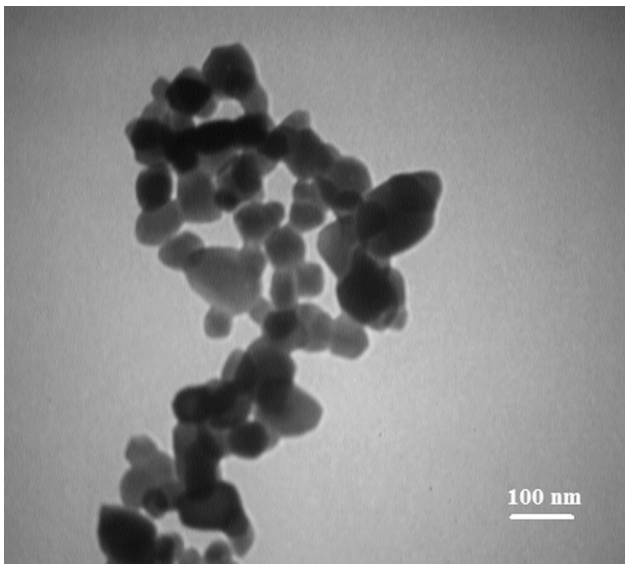

Fig. 3 TEM image of $CoWO_4$ nanoparticles prepared via precipitation under optimum conditions (run 3)

observed. These peaks are attributed to the vibrational and stretching bands of the $CoWO_4$ [18] and the peaks are in agreement with previous report which explained the main absorption bands of wolframite type structure AWO_4 (A = Co, Fe, Ni, Mn, Cd, Mg, Zn) appeared in the range of 450–1000 cm^{-1} [23, 24]. The absorption bands at 818.8 and 867.16 cm^{-1} were considered to be due to the vibration of the WO_2 units in the W_2O_8 group. The bands at 685.1 and 611.8 cm^{-1} were considered to correspond to the symmetric vibrations of the bridging O atoms of the Co–O–W, and the absorption bands at 526.2 and 466.4 cm^{-1} could be attributed to the symmetrical and asymmetrical deformations of W–O and Co–O in WO_6 and CoO_6 octahedrons [23, 24], which could be attributed to the production of $CoWO_4$. It can be seen that the $CoWO_4$ crystals were produced, which is confirmed by the pattern of XRD analysis. Thus, the results of Fig. 5 are as another evidence for formation of $CoWO_4$ as product of precipitation reaction.

The prepared cobalt tungstate nanoparticles were also characterized by UV–Vis spectrophotometry to investigate their absorption property. UV–Vis absorption spectrum of the cobalt tungstate nanoparticles dispersed in distilled water is shown in Fig. 6. As seen in this figure, the spectrum of dispersed nanoparticles shows a main absorption in the wavelength range of 200–250 nm and the absorbance decreases progressively at higher wavelengths. The UV–Vis spectrum confirms a small crystal size for the synthesized cobalt tungstate at the optimum conditions, which is due to the strong quantum confinement of the excitonic transition in nano-structures [31].

3.3 Electrochemical studies

The supercapacitive performance of the $CoWO_4$ electrode were studied by CV method, using a three-electrode system using Ag/AgCl as the reference and platinum foil as the counter-electrode. The specific capacitance (SC, F g^{-1}), of electrodes based on the recorded CVs can be estimated by the following equation [32]:

$$SC = \frac{1}{v(V_c - V_a)} \int_{V_a}^{V_c} IdV \quad (1)$$

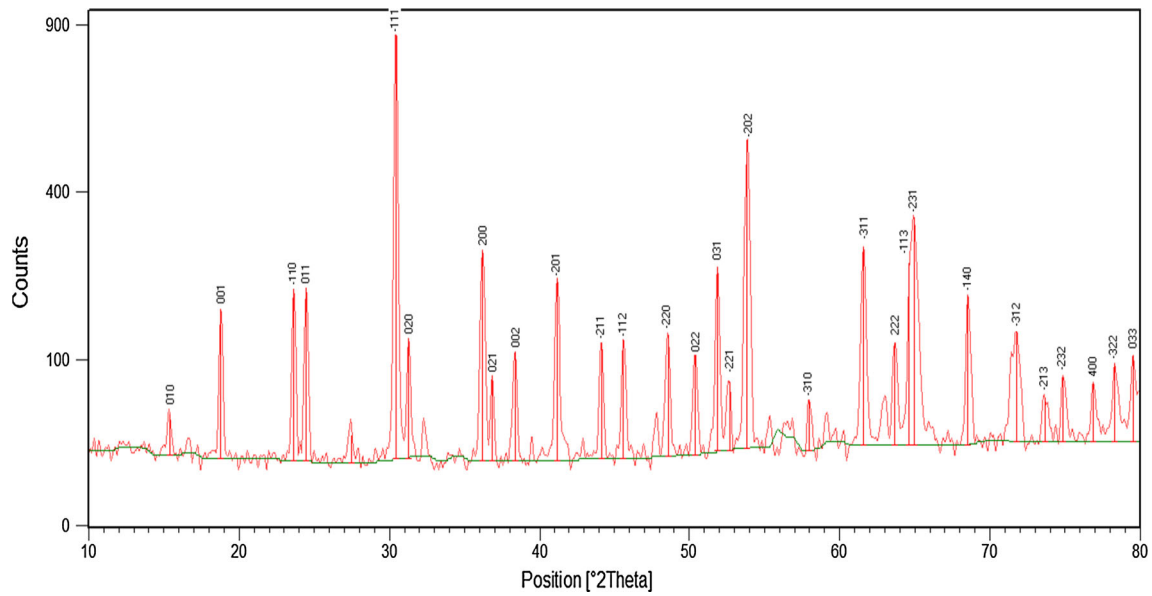

Fig. 4 XRD pattern of the synthesized $CoWO_4$ nanoparticles by precipitation method

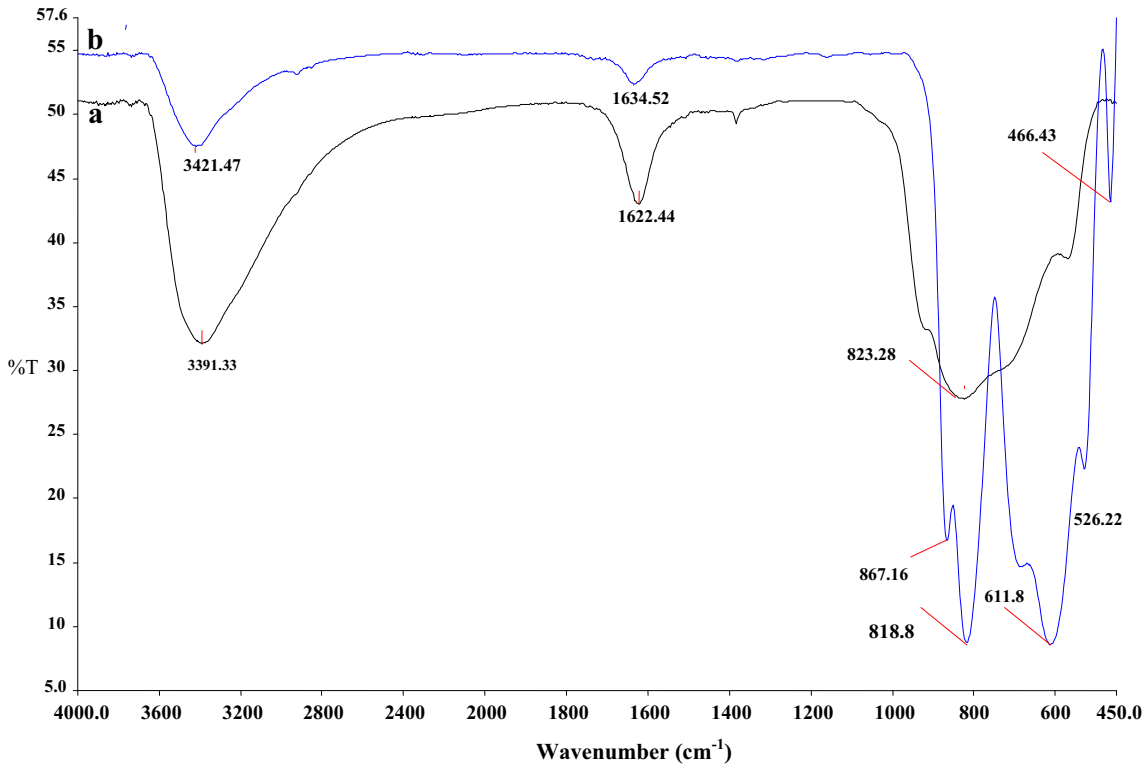

Fig. 5 FT-IR spectrum of $CoWO_4$ nanoparticles prepared via precipitation method *a* before and *b* after annealing in 600 °C

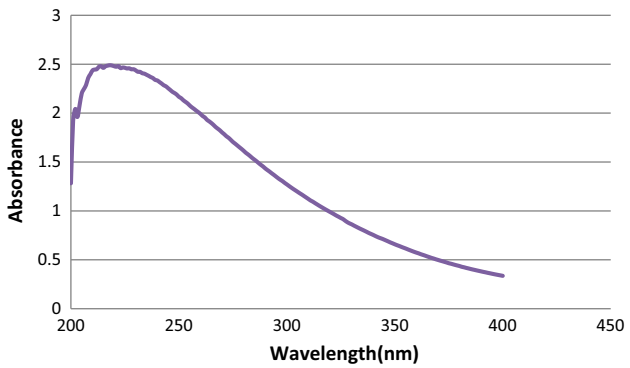

Fig. 6 UV–Vis absorption spectra of the $CoWO_4$ nanoparticles prepared via precipitation method under optimum conditions

where v is the potential scan rate (mV s^{-1}), V_c and V_a is the potential range and I denotes the response current (mA g^{-1}) based on the mass of electroactive material. Figure 7a shows the CV curves of the $CoWO_4$ electrode at the scan rates of 5, 10, 20, 30, 50, 75 and 100 mV s^{-1}, respectively. As shown, the shapes of these curves are quasi-rectangular indicating the ideal electrical double-layer capacitance behavior and the fast charge/discharge process characteristic. Figure 7b illustrates the change in the SC as a function of the scan rates for the $CoWO_4$ electrode. As shown, the SC of $CoWO_4$ electrode from 378 to 242 F g^{-1} with scan rate, from 2 to 200 mV s^{-1}. Actually, at low scan rates, the ions of the electrolyte (H^+) have enough time to enter into material's pores. This provides more available surface for effective redox reactions rather than that at high scan rates, which only the outer surface of the material is available. So, increasing the scan rate caused a decrease in the total SC.

Galvanostatic charge/discharge electrochemical measurements were used to evaluate the supercapacitive performance of the $CoWO_4$ electrode. Figure 7c illustrates the charge/discharge curves in the potential range of −0.3 to 0.4 V for the $CoWO_4$ electrode in 2.0 M H_2SO_4 solutions, at current densities ranging from 1 to 16 A g^{-1}. In this figure, all of the curves are linear, triangular-shaped, very sharp and symmetric. Besides, the durations of charging and discharging processes are almost equal for each electrode, which implies a high columbic efficiency, reversible behavior, and ideal capacitor performance.

The calculated of the SC in charge/discharge curve are calculated from discharge time using the following equation [32]:

$$SC = \frac{It_d}{mV} \tag{2}$$

where I is the charge/discharge current (A), t_d is the discharge time (s), m is the active mass (g) and V is the potential drop during discharge (V). Figure 7d shows rate

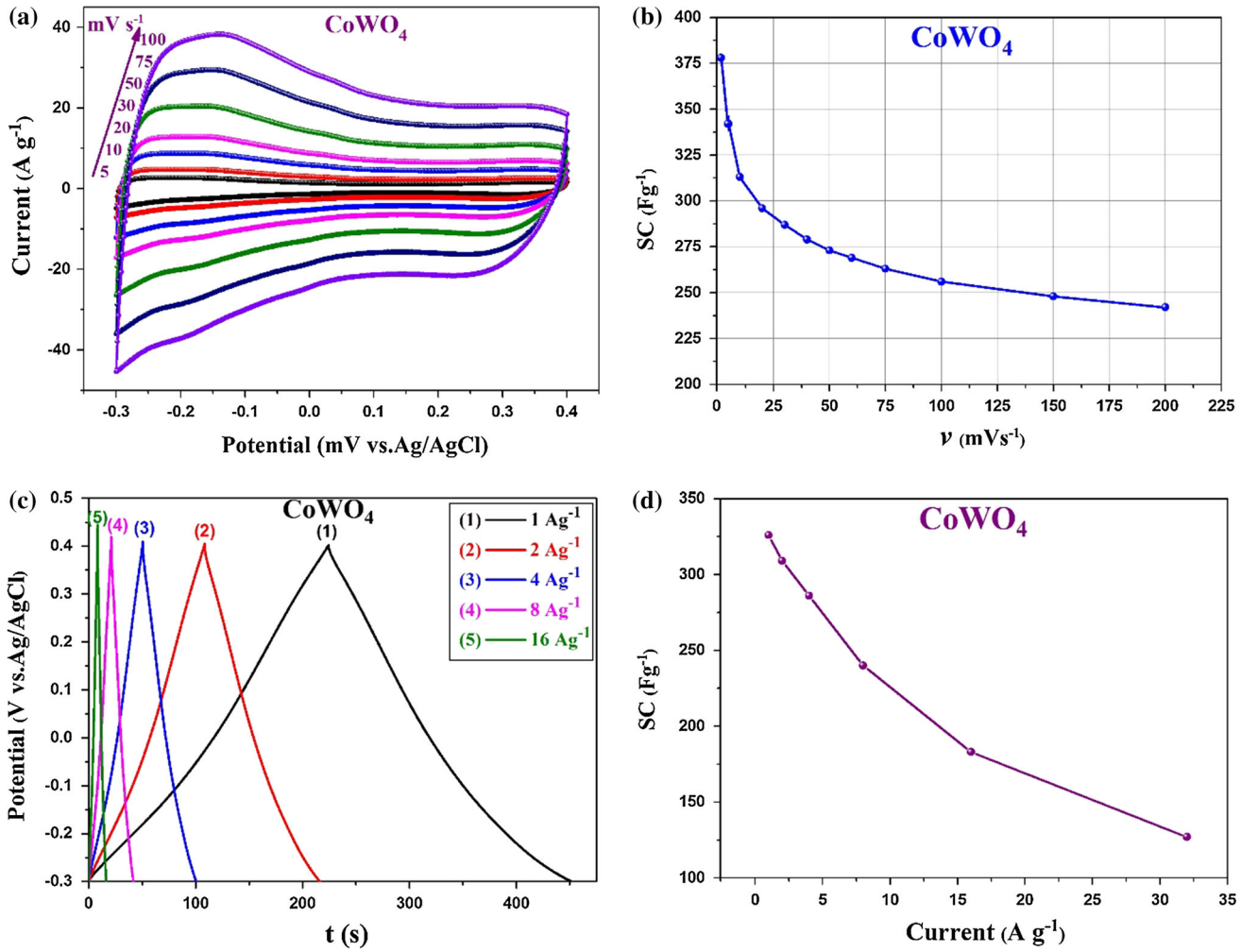

Fig. 7 **a** The CVs of $CoWO_4$ electrode at different scan rates, **b** variation of SC as a function of scan rates, **c** charge/discharge curves of $CoWO_4$ electrode at various current densities, and **d** variation of SC as a function of current

performance of the $CoWO_4$ electrode at various current densities. The SC of the $CoWO_4$ electrode decreases with the increasing current density. The SC of the $CoWO_4$ electrode was calculated to 385 F g^{-1} at the current density of 1 A g^{-1}, which is higher than those of other same reported [13–15].

Ragone plots (power density vs. energy density) of $CoWO_4$ electrode is shown in Fig. 8. The energy and power densities were derived from charge/discharge curves at various current densities and these can be calculated from the following equations [33]:

$$E = \frac{1}{2}C(\Delta V)^2 \tag{3}$$

$$P = \frac{Q\Delta V}{2t} = \frac{E}{t} \tag{4}$$

where P and E are the power density (W kg^{-1}) and energy density (W h kg^{-1}), respectively. C is the specific

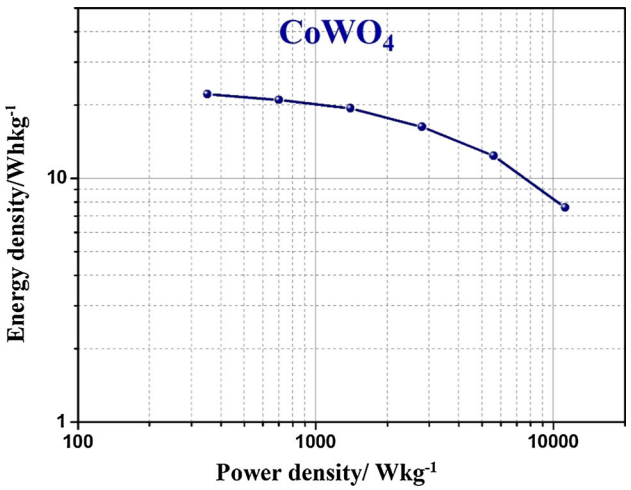

Fig. 8 Ragone plot (power density vs. energy density) of $CoWO_4$ electrode

capacitance based on the mass of the electroactive material (F g^{-1}), Q is the total charge delivered (C), ΔV is the potential window of discharge (V), and t is the discharge time (s).

As shown in Fig. 8, energy density decreases with the increase of power density. The maximum energy density obtained for the $CoWO_4$ electrode with a value of 22.2 W h kg^{-1} at the power density of 350 W kg^{-1}. Due to value of the energy density and power density, it could be stated that $CoWO_4$ electrode are suitable materials for ESs.

The CCV technique could be considered the best tools for examination of the monitoring in the CVs and charge storage of a capacitor during that time [34]. In this method, under a long-term potential cycling, the stability of the electrodes are evaluated. The calculated SC as a function of number of cycles is presented in Fig. 9a. In this curve, shows the value of SC over the number of cycles decreases slightly. Finally after 4000 cycles retain at 95.5 % of its original value, at 200 mV s^{-1} scan rate. The above results prove that the $CoWO_4$ electrode is highly stable during potential cycling test compared to other metal oxides [11–13, 16]. Figure 9b shows three-dimensional (3D) CCVs, which was performed at a scan rate of 200 mV s^{-1}. In these two 3D-plots, the changes in the CVs over number of cycles are more noticeable.

It is well known that the EIS analysis is an important method for the supercapacitive performance investigation and impedance of the electrode materials used in ESs. Figure 10 shows the Nyquist impedance plot (imaginary part, Z′, vs. real part, Z″) over the frequency range 0.01–10^5 Hz, for the $CoWO_4$ electrode in 2.0 M H_2SO_4 solutions, at potential of 0.1 V (about the midpoint of the cyclic voltammetry range). The EIS curve contains a semicircle at high frequency region and of a line in the lower frequency region. The observing a large semicircle for the entire $CoWO_4$ electrode is indication of presence of a Faradaic charge transfer resistance (R_{ct}). Based on observed the diameter of the semicircle, the calculated R_{ct} of the $CoWO_4$ electrode is 0.53 Ω. In the low frequency range, the Warburg tail is expected to occur at 45°, corresponding to the capacitor's diffusive resistance of the electrolyte in the electrode pores and the ion diffusion in the host material. Whereas, The Nyquist plot is close to vertical, which imply that the electrochemical of the electrodes is similar to an ideal capacitor. The large Warburg region (the straight line) of $CoWO_4$ electrode shows the great variations in ion diffusion path lengths and increased barrier of ion movement [33]. In point of fact, the electrode at the high frequency reflects the electrode series resistance (R_s) in the electrode/electrolyte system, which corresponds to the characteristics of both the electrolyte and electronic resistance of the electrode. The R_s of

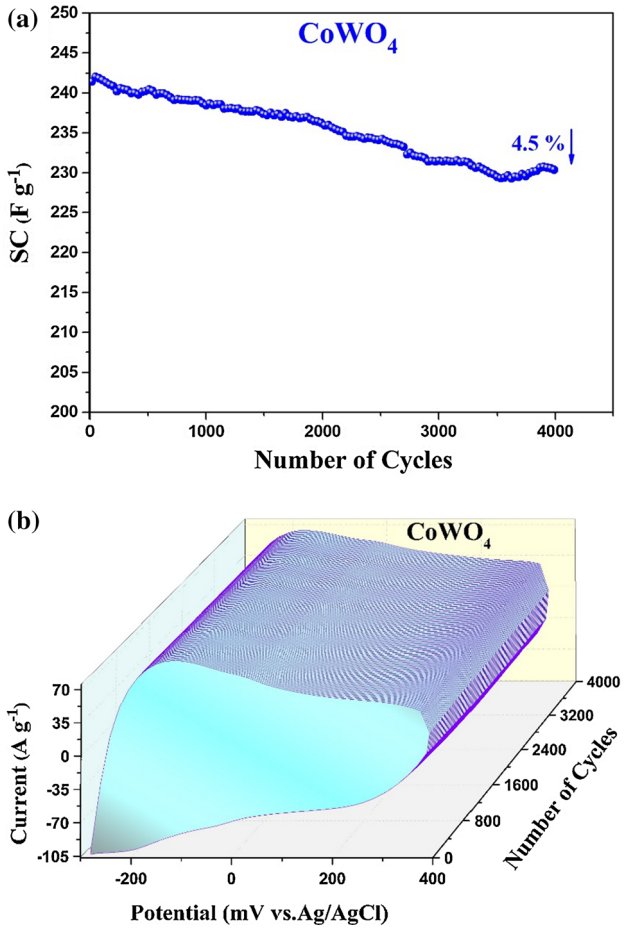

Fig. 9 **a** Variation of the SC of the $CoWO_4$ electrode as a function of number of cycles at 200 mV s^{-1}, and **b** 3D-CCV curves of the $CoWO_4$ electrode electrodes measured at scan 200 mV s^{-1}

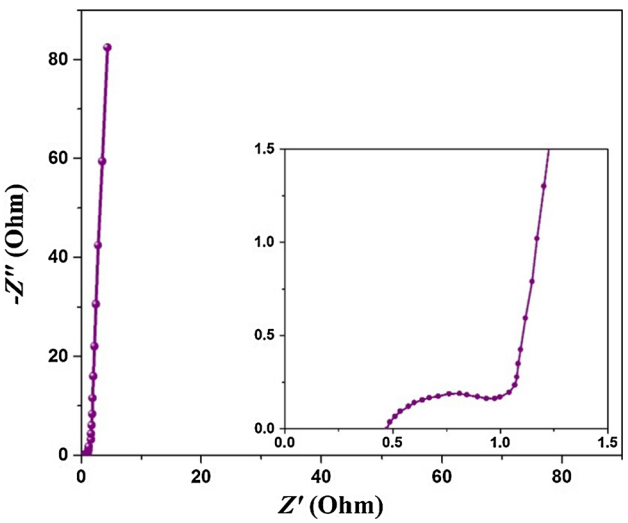

Fig. 10 EIS of $CoWO_4$ electrode in the frequency range from 0.01 Hz to 100 kHz

$CoWO_4$ electrode is obtained from the intersection of the Nyquist plot. The calculated R_s for the $CoWO_4$ electrode are 0.47 Ω. The inset in the Fig. 10 shows the expanded high frequency region of impedance.

4 Conclusion

Present study reports successful synthesis of $CoWO_4$ nanoparticles via chemical precipitation reaction as a simple, fast, and cost effective method using no template, surfactant, or catalyst. The chemical composition and morphology of the cobalt tungstate nanoparticles were characterized by various techniques i.e., SEM, XRD, UV–Vis, and FT-IR. The $CoWO_4$ electrode indicates high specific capacitance of 378 F g^{-1} at scan rate of 2 mV s^{-1} in 2.0 M H_2SO_4 electrolyte. Therefore, the prepared electrode could be potential electrode materials for supercapacitors. Moreover, an excellent rate performance, good capacitance retention ($\sim$95.5 %) was also observed during the continuous 4000 cycles.

Funding The authors are gratefully acknowledged the financial support provided by Iran National Science Foundation (Project 94019559).

References

1. B.E. Conway, *Electrochemical Supercapacitors: Scientific Fundamentals and Technological Applications* (Kluwer Academic/Plenum, New York, 1999)
2. J. Yan, Q. Wang, T. Wei, Z. Fan, Adv. Energy Mater. **4**, 1 (2013)
3. H. Luo, F. Zhang, X. Zhao, Y. Sun, K. Du, H. Feng, J. Mater. Sci. Mater. Electron. **25**, 538 (2014)
4. L. Yang, M. Li, Y. Zhang, K. Yi, J. Ma, Y. Liu, J. Mater. Sci. Mater. Electron. **25**, 1047 (2014)
5. A.G. Pandolfo, A.F. Hollenkamp, J. Power Sources **157**, 11 (2006)
6. M. Li, Y. Zhang, L. Yang, Y. Liu, J. Ma, J. Mater. Sci. Mater. Electron. **26**, 485 (2015)
7. C.D. Lokhande, D.P. Dubal, O. Joo, Curr. Appl. Phys. **11**, 255 (2011)
8. M. Mastragostino, C. Arbizzani, F. Soavi, J. Power Sources **98**, 812 (2001)
9. V.S. Kumbhar, A.D. Jagadale, N.M. Shinde, C.D. Lokhande, Appl. Surf. Sci. **259**, 39 (2012)
10. S.L. Kuo, J.F. Lee, N.L. Wu, J. Electrochem. Soc. **154**, A34 (2007)
11. U. Nithiyanantham, S.R. Ede, S. Anantharaj, S. Kundu, Cryst. Growth Des. **15**, 673 (2015)
12. S.R. Ede, A. Ramadoss, U. Nithiyanantham, S. Anantharaj, S. Kundu, Inorg. Chem. **54**, 3851 (2015)
13. S.R. Ede, S. Kundu, ACS Sustain. Chem. Eng. **3**, 2321 (2015)
14. U. Nithiyanantham, S.R. Ede, T. Kesavan, P. Ragupathy, M.D. Mukadam, S.M. Yusuf, S. Kundu, RSC Adv. **4**, 38169 (2014)
15. X. Xing, Y. Gui, G. Zhang, C. Song, Electrochim. Acta **157**, 15 (2015)
16. B. Guan, L. Hu, G. Zhang, D. Guo, T. Fu, J. Li, H. Duan, C. Li, Q. Li, RSC Adv. **4**, 4212 (2014)
17. S.M. Pourmortazavi, M. Rahimi-Nasrabadi, M. Khalilian-Shalamzari, M.M. Zahedi, S.S. Hajimirsadeghi, I. Omrani, Appl. Surf. Sci. **263**, 745 (2012)
18. S.M. Pourmortazavi, M. Rahimi-Nasrabadi, Y. Fazli, M. Mohammad-Zadeh, Int. J. Refract. Met. Hard Mater. **51**, 29 (2015)
19. Z. Song, J. Ma, H. Sun, Y. Sun, J. Fang, Z. Liu, C. Gao, Y. Liu, J. Zhao, Mater. Sci. Eng. B **163**, 62 (2009)
20. S. Rajagopal, D. Nataraj, OYu. Khyzhun, Y. Djaoued, J. Robichaud, D. Mangalaraj, J. Alloys Compd. **493**, 340 (2010)
21. S. Thongtem, S. Wannapop, T. Thongtem, Ceram. Int. **35**, 2087 (2009)
22. A. Sen, P. Pramani, J. Eur. Ceram. Soc. **21**, 745 (2001)
23. M. Rahimi-Nasrabadi, S.M. Pourmortazavi, M.R. Ganjali, Mater. Manuf. Process. **30**, 34 (2015)
24. S.M. Pourmortazavi, M. Rahimi-Nasrabadi, M. Khalilian-Shalamzari, H.R. Ghaeni, S.S. Hajimirsadeghi, J. Inorg. Organomet. Polym. Mater. **24**, 333 (2014)
25. M. Rahimi-Nasrabadi, S.M. Pourmortazavi, M.R. Ganjali, A.R. Banan, F. Ahmadi, J. Mol. Struct. **1074**, 85 (2014)
26. M. Rahimi-Nasrabadi, S.M. Pourmortazavi, M. Khalilian-Shalamzari, S.S. Hajimirsadeghi, M.M. Zahedi, Cent. Eur. J. Chem. **11**, 1393 (2013)
27. S.M. Pourmortazavi, M. Rahimi-Nasrabadi, A.A. Davoudi-Dehaghani, A. Javidan, M.M. Zahedi, S.S. Hajimirsadeghi, Mater. Res. Bull. **47**, 1045 (2012)
28. M. Rahimi-Nasrabadi, S.M. Pourmortazavi, A.A. Davoudi-Dehaghani, S.S. Hajimirsadeghi, M.M. Zahedi, Cryst. Eng. Commun. **15**, 4077 (2013)
29. M. Rahimi-Nasrabadi, S.M. Pourmortazavi, M. Khalilian-Shalamzari, J. Mol. Struct. **1083**, 229 (2015)
30. Mehdi Rahimi-Nasrabadi, Mohsen Behpour, Ali Sobhani-Nasab, S. Mostafa Hosseinpour-Mashkani, J. Mater. Sci. Mater. Electron. **26**, 9776 (2015)
31. M. Rahimi-Nasarabadi, J. Nanostruct. **4**, 211 (2014)
32. H.R. Naderi, H.R. Mortaheb, A. Zolfaghari, J. Electroanal. Chem. **719**, 98 (2014)
33. A. Zolfaghari, H.R. Naderi, H.R. Mortaheb, Electroanal. Chem. **697**, 60 (2013)
34. A.S. Dezfuli, M.R. Ganjali, H.R. Naderi, P. Norouzi, RSC Adv. **5**, 46050 (2015)